Optical study of narrow band gap $InAs_xSb_{1-x}$ ($x = 0, 0.25, 0.5, 0.75, 1$) alloys

Shirin Namjoo*
Department of Physics, University of Isfahan, Hezar Jarib Street, Isfahan 81746-73441, Iran
and University of Graz, Institute of Physics, NAWI Graz, Universitätsplatz 5, 8010 Graz, Austria

Amir S. H. Rozatian†
Department of Physics, University of Isfahan, Hezar Jarib Street, Isfahan 81746-73441, Iran

Iraj Jabbari
Faculty of New Sciences and Technology, University of Isfahan, Hezar Jarib Street, Isfahan 81746-73441, Iran

Peter Puschnig
University of Graz, Institute of Physics, NAWI Graz, Universitätsplatz 5, 8010 Graz, Austria
(Received 4 March 2015; revised manuscript received 28 April 2015; published 13 May 2015)

The structural, electronic, and optical properties of InAs, InSb, and their ternary alloys $InAs_xSb_{1-x}$ ($x = 0.25$, 0.5, 0.75) are investigated within density functional theory utilizing the WIEN2K package. We find that the lattice constants and bulk moduli as a function of x are in best agreement with Vegard's linear rule. When computing the electronic band structures with the modified Becke-Johnson exchange-correlation functional (mBJLDA), our results for the band gaps of InAs, InSb, and their ternary alloys are in good agreement with the available experimental results while the conventional Wu-Cohen generalized gradient approximation (GGA) functional leads to zero or close to zero band gaps. In particular, our mBJLDA results confirm experimental evidence that the minimum band gap occurs for As concentrations around $x \approx 0.3$. Furthermore, we investigate the dielectric function of these compounds within the random phase approximation using both the Wu-Cohen GGA and the mBJLDA functionals. While the mBJLDA results of our fully first-principles calculations show good agreement of the peak positions in $\epsilon_2(\omega)$ with experiments, the peaks in the optical spectra based on the Wu-Cohen GGA band structure appear redshifted compared to experiment. We further identify the interband transitions responsible for the structures in the spectra. Looking at the optical matrix element, we note that the major peaks are dominated by transition from the Sb $5p$ (As $4p$) states to In s states for InSb and $InAs_{0.25}Sb_{0.75}$ (InAs, $InAs_{0.75}Sb_{0.25}$, and $InAs_{0.5}Sb_{0.5}$).

DOI: 10.1103/PhysRevB.91.205205 PACS number(s): 71.15.Mb, 71.15.Nc, 71.20.Nr

I. INTRODUCTION

InAs ($E_g = 0.42$ eV) and InSb ($E_g = 0.24$ eV) [1] are narrow band gap semiconductors with a zinc-blende structure and space group $F\bar{4}3m$ (No. 216). Moreover, the ternary $InAs_xSb_{1-x}$ alloys have the lowest band gaps among all III-V semiconductors [2]. Due to their small direct band gaps, InAs, InSb, and their ternary alloys are important materials for a variety of midinfrared optoelectronic devices, including lasers and photodetectors [3,4]. Studies of their basic properties are very important for the understanding of device characteristics and the improvement of their performance. Previous theoretical and experimental studies on $InAs_xSb_{1-x}$ ($x = 0.25, 0.5, 0.75$) alloys were mostly limited to their electronic and structural properties [5–12]. Experimental results on optical properties were mainly restricted to the optical band gap, but a full measurement of the frequency-dependent dielectric function has yet to be conducted, except for InAs and InSb [13]. Theoretically, the dielectric function has also only been computed for InAs and InSb [14]. But to the best of the authors' knowledge, experimental and theoretical results on the dielectric function of $InAs_xSb_{1-x}$ alloys are still lacking. These compounds are particularly interesting since the presently available experimental data suggest a minimum in the band gap for concentrations around $x \approx 0.3$. Therefore, the goal of this study is to investigate these findings further and to characterize the optical properties of these alloys completely by computing the frequency-dependent dielectric function.

The paper is organized as follows. A brief summary of the computational method is presented in Sec. II. The results are presented and discussed in Sec. III. There, we first study the structural properties and electronic band structures of InSb, InAs, and also $InAs_xSb_{1-x}$ ($x = 0.25, 0.5, 0.75$) alloys and compare the results with the previous studies. Then, we investigate the dielectric function of InSb, InAs, and their ternary alloys within the random phase approximation. The article ends with the conclusions.

II. COMPUTATIONAL DETAILS

All calculations presented in this work were performed within the framework of density functional theory (DFT) utilizing the full potential linearized augmented plane wave method (FP-LAPW) [15,16] as implemented in the package WIEN2K [17]. Spin-orbit coupling is included by a second variational procedure [15], where states up to 9 Ry above the Fermi energy are included in the basis expansion. The equilibrium lattice constants were determined by total energy minimization using the generalized gradient approximation (GGA) functional according to Wu and Cohen [18]. The

*namjoo_sh@yahoo.com
†a.s.h.rozatian@phys.ui.ac.ir

TABLE I. Lattice parameter and bulk modulus of InAs, InSb, and $InAs_xSb_{1-x}$ ($x = 0.25, 0.5, 0.75$) alloys.

	Lattice constant a (Å)			Bulk modulus B (GPa)		
x	Our work	Expt.	Other calc.	Our work	Expt.	Other calc.
0	6.536	6.479[a]	6.346[b], 6.635,[c] 6.341,[d] 6.476[e]	42.96	48.3[a]	47.6,[b] 36.73,[c] 47.74,[d] 46.8[e]
0.25	6.423		6.537[c]	45.312		40.123[c]
0.5	6.313		6.435[c]	48.96		43.559[c]
0.75	6.209		6.310[c]	52.28		46.468[c]
1	6.099	6.058[a]	5.921,[b] 6.192,[c] 5.902,[d] 6.051[e]	56.181	58[a]	61.7,[b] 48.69,[c] 61.7,[d] 60.3[e]

[a]Reference [1].
[b]Reference [10].
[c]Reference [11].
[d]Reference [6].
[e]Reference [7].

basis set convergence parameter $R_{MT}^{min}K_{max}$ (the product of the smallest of the atomic sphere radii R_{MT}^{min} and plane wave cutoff parameter K_{max}) was set to 9. The maximum l quantum number for the wave function expansion inside the atomic sphere was confined to $l_{max} = 10$. The G_{max} parameter was taken to be 12.0 bohr^{-1}. Brillouin-zone (BZ) integrations within the self-consistency cycles were performed with the tetrahedron method [19], using 3000 (1000) k points in the full BZ points for the binary compounds (ternary alloys), while denser meshes of 10 000 (7000) k points for binary compounds (ternary alloys) have been used for optical properties. All of these values were chosen so as to ensure convergence of the results. The force on each atom after relaxation decreased to less than 0.5 mRyd/a.u. For the computation of the band structures, the modified Becke-Johnson exchange potential together with local-density approximation for the correlation potential (mBJLDA) [20] was used. The mBJLDA potential offers an improvement over LDA [21,22] or GGA [23] in describing band gaps of many materials, including semiconductors with the zinc-blende structure, leading to an experimental agreement comparable to hybrid functional or *GW* calculations [20]. Note, however, that the mBJLDA potential has no corresponding definition about its energy functional and therefore cannot be used for structural optimizations.

III. RESULTS AND DISCUSSION

A. Structural properties

Both InAs and InSb are semiconductors exhibiting the zinc-blende structure. The ternary $InAs_xSb_{1-x}$ ($x = 0.25, 0.5, 0.75$) alloys are in fact pseudobinary alloys in which the As and Sb atoms are placed on the As/Sb sublattice. In our work, we have only considered ordered alloys for $x = 0.25$, 0.5, and 0.75, resulting in the smallest possible supercells. For $InAs_{0.25}Sb_{0.75}$ and $InAs_{0.75}Sb_{0.25}$, we have chosen an eight-atom simple cubic lattice in which the cations with the lower concentration form a regular simple cubic lattice. For $InAs_{0.5}Sb_{0.5}$, the smallest ordered structure is a four-atom tetragonal cell for which we relax the a and c parameters separately, leading to $a = 4.464$ and $c = 6.322$, which shows that the tetragonal distortion of the original cubic structure is only 0.1%. We emphasize that in this work the effects of disorder on the As-Sb sublattice have not been considered. This could be the subject of future investigations. We have computed the lattice constants and bulk moduli for InAs, InSb, and the three alloy compositions $InAs_xSb_{1-x}$ ($x = 0.25, 0.5, 0.75$) by total energy minimization within the Wu-Cohen GGA [18]. The results are summarized in Table I, together with other theoretical results from literature and the available experimental data.

For InAs and InSb, the calculated lattice parameters and bulk moduli are generally in good agreement with experiment. Our lattice parameters for InAs and InSb only slightly overestimate the experimental values by 0.7% and 0.9%, respectively. A similar level of accuracy is expected for the ternary alloys where experimental data for the specific concentrations treated by us were missing. Also our computed bulk moduli are only fairly underestimated by 3% and 11% for InAs and InSb when compared to measurements. Note that our results are also in agreement with previous DFT calculations. The deviations can be explained by the usage of different exchange-correlation functionals or the computational schemes. For instance, Hachelafi *et al.* [11] were using the Perdew-Burke-Ernzerhof (PBE)-GGA functional [23] for their FP-LAPW results for $InAs_xSb_{1-x}$ ($x = 0.25, 0.5, 0.75$) alloys, while we were using the Wu-Cohen GGA functional [18], which leads to slightly better agreement with experiment.

When plotting the lattice parameter and bulk modulus as a function of x (Fig. 1), we find an almost perfect linear behavior showing that Vegard's linear rule [24] can be an excellent

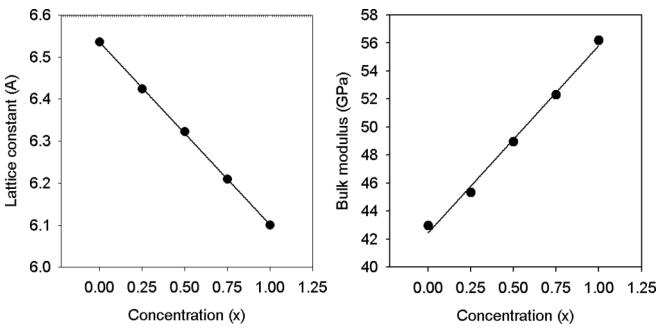

FIG. 1. Lattice constant (left) and bulk modulus (right) vs composition (x) for InSb, $InAs_xSb_{1-x}$ ($x = 0.25$, 0,5, 0,75) alloys, and InAs. The solid curves are linear fits to the data points given by $a = 6.536 - 0.435x$ and $B = 42.456 + 13.364x$.

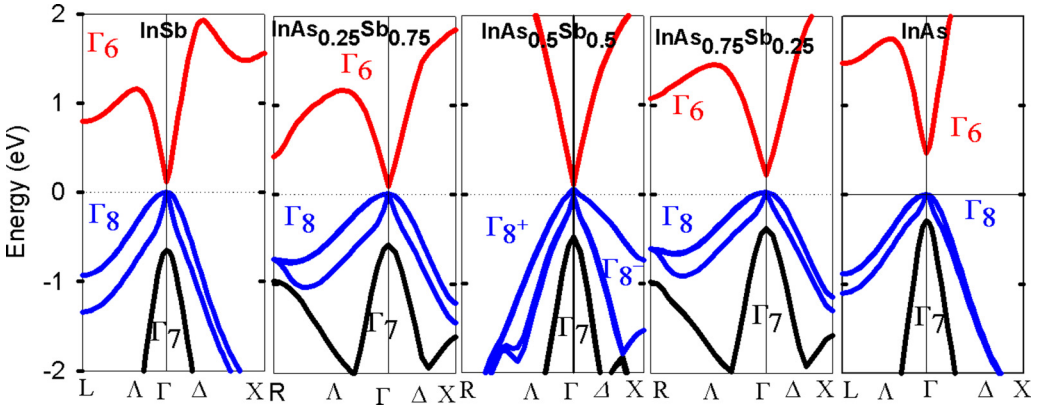

FIG. 2. (Color online) The calculated band structures of InAs, InSb, and $InAs_xSb_{1-x}$ ($x = 0.25$, 0,5, 0,75) alloys using the mBJLDA functional [26]. The different colors are used to distinguish bands of different symmetry.

approximation to obtain the lattice constants and also bulk moduli of $InAs_xSb_{1-x}$ alloys. As expected, due to the larger atomic radius of Sb compared to As, the lattice parameter decreases with the As concentration x, while the bulk modulus linearly increases as we go from InSb to InAs, showing that InSb is more compressible than InAs.

B. Electronic band structures

As mentioned in the Introduction, InAs and InSb are narrow band gap semiconductors exhibiting the zinc-blende structure. Their energy bands at the Γ point near the Fermi level can be characterized according to the cubic symmetry as Γ_6 (twofold degenerate), Γ_7 (twofold degenerate), and Γ_8 (fourfold degenerate) states where the splitting of the valence band maximum is due to a spin-orbit interaction [25]. The Γ_8 states ($j = 3/2$) at the Fermi level have p-like symmetry, while the valence level Γ_6 has s-like symmetry. The spin-orbit splitting is characterized by the energy difference between Γ_8 and Γ_7 states which we denote by ΔSO.

As mentioned in the previous section, for $InAs_{0.25}Sb_{0.75}$ and $InAs_{0.75}Sb_{0.25}$, the simplest structure is an eight-atom simple cubic lattice while for $InAs_{0.5}Sb_{0.5}$, the smallest ordered structure is a four-atom tetragonal cell. Because of the cubic symmetry in $InAs_{0.25}Sb_{0.75}$ and $InAs_{0.75}Sb_{0.25}$, the characters of the bands around Γ are similar to their parent compounds InAs and InSb, while due to the tetragonal symmetry in $InAs_{0.5}Sb_{0.5}$, the degeneracy of the fourfold degenerate Γ_8 is lifted, and a small energy gap of 0.07 eV is opened between the Γ_8^+ state (higher energy) and the Γ_8^- state (lower energy) at the Γ point. The band structures of InAs, InSb, and also $InAs_xSb_{1-x}$ ($x = 0.25$, 0.5, 0.75) alloys are shown in Fig. 2.

As seen in Fig. 2, InAs, InSb, and their ternary alloys for all considered concentrations of As are direct band gap semiconductors. The calculated values of the band gap of InAs, InSb, and $InAs_xSb_{1-x}$ ($x = 0.25$, 0.5, 0.75) alloys using the mBJLDA functional are shown in Table II and also depicted in Fig. 3. Note that the usage of the Wu-Cohen GGA functional leads to zero band gaps for all compounds with cubic symmetry and to gap of only ≈0.009 eV for $x = 0.5$. Most notably, the band gap as a function of concentration shows a strong deviation from linearity. In particular, our data suggest a minimum for concentrations between $x = 0.25$ and 0.50. When fitting a second-order polynomial to our data points, we predict a band gap minimum at an As concentration of $x = 0.32$. This number is in excellent agreement with the values of $x = 0.35$ [27] and $x = 0.36$ [28] obtained from photoluminescence (PL) measurements. The bowing parameter b, which expresses the deviation from linearity, is calculated to be 0.92 eV. This value should be compared to the bowing parameter of $InAs_xSb_{1-x}$ alloys estimated from low temperature PL measurements which was reported to be 0.672 [27] and 0.6853 eV [28] at 0 K. To our knowledge, there is only one theoretical work in which the band gap bowing of the $InAs_xSb_{1-x}$ alloys has been calculated [12]. Using an empirical tight binding method, the authors of Ref. [12] have obtained a band gap bowing parameter of 1.72 eV, which is almost twice as large as our value and almost three times as large as the experimental values. Note that in the DFT work of Hachelafi *et al.* [11], their usage of the PBE-GGA functional for the discussion of the band structures has led to zero band gap semiconductors and no dependence of the band gap on the As concentration was presented.

Table II and Fig. 3 also display the spin-orbit splitting ΔSO versus alloy composition. One of the important effects of increasing the As content in InSb is the reduction of the spin-orbit coupling strength. This can be easily understood since the spin-orbit coupling generally increases with the atomic number. Thus, with increasing the As content in InSb, ΔSO decreases. The values of spin-orbit coupling for binary compounds are in good agreement with the results of angle-resolved photoemission experiments, i.e., 0.39 eV (InAs) and

TABLE II. Calculated band gap (E_g) and spin-orbit splitting (ΔSO) of InAs, InSb, and $InAs_xSb_{1-x}$ ($x = 0.25$, 0.5, 0.75) using the mBJLDA functional.

x	E_g (eV)	$\Delta SO = E_{\Gamma_8} - E_{\Gamma_7}$
0	0.122	0.648
0.25	0.082	0.575
0.5	0.048	0.462
0.75	0.196	0.404
1	0.470	0.296

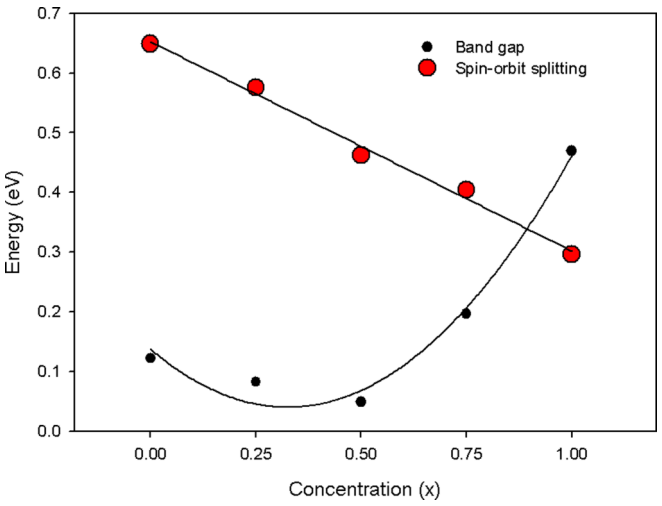

FIG. 3. (Color online) The band gap and spin-orbit splitting vs composition (x) for InAs, InSb, and $InAs_xSb_{1-x}$ alloys ($x = 0.25$, 0.5, 0.75). The solid curves are fits given by the quadratic expression $E_g = 0.1373 - 0.6005x + 0.9244x^2$ and the linear expression $\Delta SO = 0.653 - 0.350x$.

0.81 eV (InSb) [2]. According to the figure, the deviation of calculated spin-orbit splitting versus concentration from linearity is relatively small.

C. Optical properties

The optical properties of materials can be described by means of the transverse dielectric function $\epsilon(\omega)$. There are two contributions to $\epsilon(\omega)$, namely, intraband and interband transitions. In the limit of 0 K, the contribution from the intraband transitions is only relevant for metals. The interband transitions can further be split into direct and indirect transitions. Here, we neglect the indirect interband transitions which involve scattering of phonons and are expected to give only a small contribution to $\epsilon(\omega)$ [29,30]. To calculate the direct interband contribution to the imaginary part of the dielectric function $\epsilon(\omega)$, one must sum over all possible transitions from occupied to unoccupied states. By taking the appropriate transition matrix elements into account, the imaginary part of the dielectric function within the random phase approximation (RPA) and neglecting local field effects is given by

$$\epsilon_2(\omega) = \frac{\upsilon e^2}{2\pi\hbar m^2\omega^2}\int d^3k \sum_{nn'} |\langle k_n|p|k_{n'}\rangle|^2 f(k_n) \times [1 - f(k_{n'})]\delta(E_{k_n} - E_{k_{n'}} - \hbar\omega). \quad (1)$$

Here $\hbar\omega$ is the energy of the incident photon, p is the momentum operator, $|k_n\rangle$ are the eigenfunctions with eigenvalues E_{k_n}, and $f(k_n)$ is the Fermi distribution function. A detailed description of the calculation of these matrix elements is given by Ambrosch-Draxl *et al.* [30]. From the imaginary part of the dielectric function, the real part of the dielectric function is obtained by use of the Kramers-Kronig relations [31]. The dielectric function is a symmetric tensor of second rank with up to six independent components, according to the symmetry of the crystal. In the case of cubic symmetry, the optical properties are isotropic, i.e., there is only one independent component, while for uniaxial symmetry (tetragonal, hexagonal) there are two independent components.

In order to allow for a better comparison of the optical spectra with the underlying band structures, Fig. 4 shows the imaginary parts of dielectric function for InAs and InSb, together with their band structure. For the dielectric function, we include both results for the mBJLDA functional (solid lines) and for the Wu-Cohen functional (dashed lines) where the latter are redshifted with respect to the former, owing to the underestimation of the band gap in the Wu-Cohen functional. Note that the same trend is observed also for the ternary alloys, as can be seen from Fig. 5.

Therefore, in the following discussion, we focus on the mBJLDA results, and, in particular, discuss three major peaks of $\epsilon_2(\omega)$ which we denote by a, b, and c. It is worthwhile to attempt to identify the transitions that are responsible for the structures in $\epsilon_2(\omega)$ using our calculated band structures. According to the optical matrix elements, it is found that for InSb (InAs), the Sb $5p$ (As $4p$) states and In s states play a major role in these optical transitions as the initial and final states. For both InSb and InAs, peak a arises from transitions between the highest valence bands (27th, 28th) and the lowest conduction bands (29th, 30th) around the L point in the BZ. Peak b, which originates from the spin-orbit effects, is due

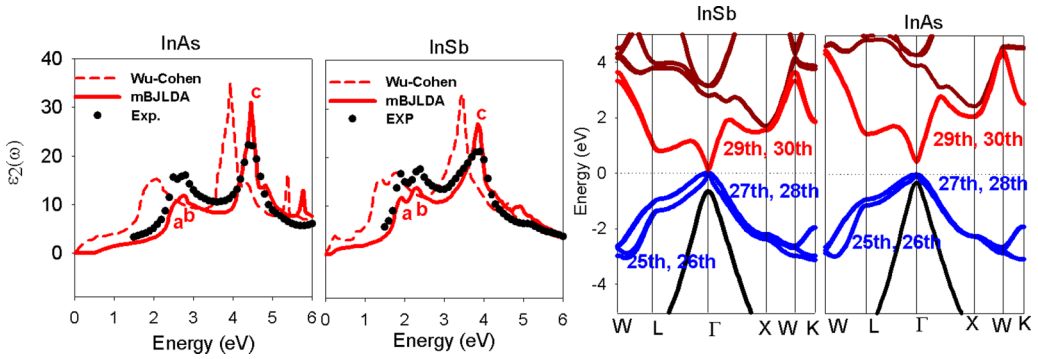

FIG. 4. (Color online) Calculated band structures (right) and imaginary parts of the dielectric function (left) of InAs and InSb. The red solid (dashed) lines are our calculations using the mBJLDA (Wu-Cohen GGA) functional while the black circles depict the available experimental results [13].

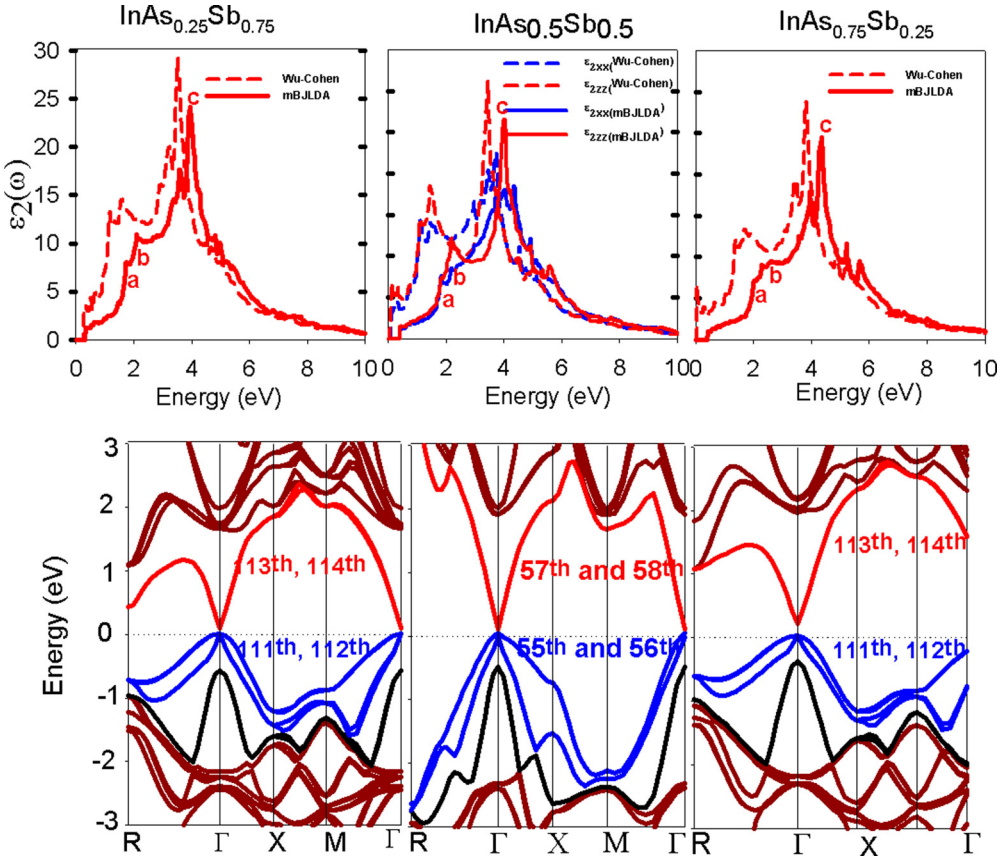

FIG. 5. (Color online) Top panels: Calculated imaginary parts of dielectric function for $InAs_{0.25}Sb_{0.75}$, $InAs_{0.5}Sb_{0.5}$, and $InAs_{0.75}Sb_{0.25}$ from left to right. Dashed lines are based on the Wu-Cohen functional, while the solid lines result from the mBJLDA functional. Bottom panels: Corresponding electronic band structures.

to transitions from the 25th and 26th bands to the lowest conduction bands (29th, 30th) from the points in BZ around the L point.

Peak c for these binary compounds is also related to the transition from the highest valence bands to the lowest conduction bands, however, arising from transitions near the X point of the BZ. Note that the positions of all three peaks a, b, and c match very nicely with the experimental results [13] and are in better agreement than the other theoretical work which is related to the optical properties of InAs and InSb [14]. The remaining difference between our results and experiment concerns mainly the oscillator strengths of the transitions. While our calculations underestimate the height of peaks a and b, they overestimate the transition strength of peak c. This behavior may arise from excitonic effects that have not been considered in our work [32,33].

We now focus on the optical properties of the ternary alloys $InAs_{0.25}Sb_{0.75}$, $InAs_{0.5}Sb_{0.5}$, and $InAs_{0.75}Sb_{0.25}$, which are presented in Fig. 5, together with the corresponding band structures. In analogy to the the parent compounds InAs and InSb, we can identify three major peaks denoted by a, b, and c, which are dominated by transitions from Sb $5p$ (As $4p$) states to In s states for $InAs_{0.25}Sb_{0.75}$ ($InAs_{0.75}Sb_{0.25}$ and $InAs_{0.5}Sb_{0.5}$). We note that all the structures in the imaginary part of the dielectric function are shifted towards lower energies as we go from $InAs_{0.75}Sb_{0.25}$ to $InAs_{0.25}Sb_{0.75}$. This trend is directly inferred from the band structure results. As we go from $InAs_{0.75}Sb_{0.25}$ to $InAs_{0.25}Sb_{0.75}$, the band

TABLE III. Position of peak a and dominant contributions to this peak with available experimental values in parentheses for InAs, InSb, and $InAs_xSb_{1-x}$ ($x = 0.25, 0.5, 0.75$).

x	Calculated peak position (expt.) (eV)	From bands to bands
0	1.92 (1.9)	27,28 → 29,30
0.25	1.75	111,112 → 113,114
0.5	1.84	55,56 → 57,58
0.75	2.02	111,112 → 113,114
1	2.46 (2.5)	27,28 → 29,30

TABLE IV. Position of peak b and dominant contributions to this peak with some experimental values for InAs, InSb, and $InAs_xSb_{1-x}$ ($x = 0.25, 0.5, 0.75$).

x	Calculated peak position (expt.) (eV)	From bands to bands
0	2.33 (2.4)	25,26 → 29,30
0.25	1.75	109,110 → 113,114
0.5	2.16	53,54 → 57,58
0.75	2.3	109,110 → 113,114
1	2.76 (2.8)	25,26 → 29,30

TABLE V. Position of peak c and dominant contributions to this peak with some experimental values for InAs, InSb, and $InAs_xSb_{1-x}$ ($x = 0.25, 0.5, 0.75$).

x	Calculated peak position (expt.) (eV)	From bands to bands
0	3.82 (3.9)	27,28 → 29,30
0.25	3.96	105,106 → 115,116
0.5	4.01	55,56 → 57,58
0.75	4.36	105,106 → 115,116
1	4.45 (4.4)	27,28 → 29,30

gap decreases and this is the reason why the major peaks shift toward lower energies by going from $InAs_{0.75}Sb_{0.25}$ to $InAs_{0.25}Sb_{0.75}$. Peak a (b) for $InAs_{0.25}Sb_{0.75}$ and $InAs_{0.75}Sb_{0.25}$ is due to transitions from the 111th and 112th (109th and 110th) bands to the lowest conduction bands (113th, 114th). Peak c is related to transition from the 105th and 106th bands to 115th and 116th bands, the first and second bands above the lowest conduction bands. For $InAs_{0.5}Sb_{0.5}$, peaks a and c (b) arise from transitions between the 55th and 56th (53th and 54th) bands and the lowest conduction bands (57th, 58th). The location of the major peaks in $\epsilon_2(\omega)$, together with the available experimental results and also the dominant contribution from interband transitions for each peak, are summarized in Tables III–V. As seen in these tables, the variation of the peak position versus alloy composition for peaks a and b is nonlinear, while for peak c these positions increase linearly with the alloy concentration. The splitting of the highest valence bands at the L point for both InAs and InSb is equal to the energy difference between the positions of peaks a and b, and this splitting originates from the spin-orbit interaction. According to these tables, all major structures are shifted toward lower energy as we go from InAs to InSb. The origin of this behavior can be related to the reduction of the energy band gap as we go from InAs to InSb.

Now we turn to the static dielectric constant which are computed via a Kramers-Kronig transform of the imaginary part. The static dielectric constants of InSb, $InAs_{0.25}Sb_{0.75}$, $InAs_{0.5}Sb_{0.5}$, $InAs_{0.75}Sb_{0.25}$, and InAs are found to be 13.77, 13.16, 12.3 for $\epsilon_{0,xx}$, 12.8 for $\epsilon_{0,zz}$, and 11.7 and 10.6, respectively. The comparison of our static dielectric constants of InAs ($\epsilon_0 = 10.6$) and InSb ($\epsilon_0 = 13.77$) with room temperature measurements, $\epsilon_0 = 15.15$ for InAs and $\epsilon_0 = 17.9$ for InSb [34,35], shows that we get a similar increase when going from InAs to InSb, but underestimate the dielectric constant by roughly 25% for both binary alloys. The increase from InAs to InSb is related to the reduction in the band gap and the deviations to the experimental values may be related to the neglect of temperature effects in our theoretical results. For $InAs_xSb_{1-x}$ ($x = 0.25, 0.5, 0.75$), experimental results for static dielectric constants to compare with are still lacking. The imaginary parts of the dielectric functions for $InAs_{0.25}Sb_{0.75}$, $InAs_{0.5}Sb_{0.5}$, and $InAs_{0.75}Sb_{0.25}$ with their band structures are shown in Fig. 5.

IV. CONCLUSIONS

We have systematically investigated the structural, electronic, and optical properties of InAs, InSb, and the ternary $InAs_xSb_{1-x}$ ($x = 0.25, 0.5, 0.75$) alloys. The calculated structural parameters obtained with the Wu-Cohen GGA functional are found to be in good agreement with the available theoretical and experimental works. Both the lattice parameter as well as the bulk modulus show a linear trend as a function of alloy concentration x. For the computation of the band structure and optical properties, we employ the mBJLDA exchange-correlation potential and take into account spin-orbit interactions in a second variational approach. The calculated mBJLDA band gaps are in good agreement with available experimental values, while our calculated Wu-Cohen GGA values severely underestimate the band gaps. For the mBJLDA functional, we obtain a strongly nonlinear behavior of the band gap as a function of alloy concentration. Out of our investigated alloy concentrations, the $InAs_{0.5}Sb_{0.5}$ yields the smallest band gap value of $E_g = 0.0484$ eV. When fitting a quadratic polynomial to our data points, we find the following dependence on the alloy concentration, $E_g = 0.1373 - 0.6005x + 0.9244x^2$, which shows a minimum in the vicinity of $x = 0.32$. This value is in excellent agreement with the experimental results.

Regarding the optical properties of $InAs_xSb_{1-x}$ ($x = 0.25$, 0.5, 0.75) alloys, we have computed the imaginary part of the dielectric function within the random phase approximation using both the Wu-Cohen and the mBJLDA functional. Overall, we find that the mBJLDA optical spectra are in excellent agreement with experiment, while the optical spectra based on the Wu-Cohen GGA functional appear redshifted. Focusing on the mBJLDA results, we find that the Sb $5p$ (As $4p$) states and In s states play a major role in low-energy optical transitions as the initial and final states for InSb and $InAs_{0.25}Sb_{0.75}$ (InAs, $InAs_{0.75}Sb_{0.25}$, and $InAs_{0.5}Sb_{0.5}$). For the binary compounds, we identify three major peaks in the optical spectrum and analyze them with respect to the bands involved in the transitions and their origin in the Brillouin zone. For these binary compounds and the ternary alloys, the lowest-energy transition consists of two subpeaks due to spin-orbit splitting and shows a nonlinear energy shift with an alloy concentration similar to the band gap, while the third peak shows a linear dependence on x. When comparing the positions of these main peaks of imaginary parts of the dielectric function for InAs and also InSb to the available experimental values, we find a perfect agreement. To our knowledge, earlier studies on the optical properties of $InAs_{0.25}Sb_{0.75}$, $InAs_{0.5}Sb_{0.5}$, and $InAs_{0.75}Sb_{0.25}$ alloys are missing. Thus, our calculations can be viewed as a prediction which can be tested against experiment in future work. The computation of the real part of the dielectric function via a Kramers-Kronig transform yields static dielectric constants of 13.77, 13.16, 12.3 for $\epsilon_{0,xx}$, 12.8 for $\epsilon_{0,zz}$, and 11.7 and 10.6 for InSb, $InAs_{0.25}Sb_{0.75}$, $InAs_{0.5}Sb_{0.5}$, $InAs_{0.75}Sb_{0.25}$, and InAs, respectively.

ACKNOWLEDGMENTS

The authors would like to thank the Office of Graduate Studies of the University of Isfahan for their support. Also we would like to thank the Ministry of Science, Research and Technology of Iran for their financial support.

[1] O. Madelung, *Semiconductors: Data Handbook* (Springer, Berlin, 2004).

[2] I. Vurgaftman, J. R. Meyer, and L. R. Ram-Mohan, J. Appl. Phys. **89**, 5815 (2001).

[3] P. Tang, M. J. Pullin, S. J. Chung, C. C. Phillips, R. A. Stradling, A. G. Norman, Y. B. Li, and L. Hart, Semicond. Sci. Technol. **10**, 1177 (1995).

[4] W. Dobbelaere, J. De Boeck, P. Heremans, R. Mertens, G. Borghs, W. Luyten, and J. Van Landuyt, Appl. Phys. Lett. **60**, 3256 (1992).

[5] J. C. Woolley and J. Warner, Can. J. Phys. **42**, 1879 (1964).

[6] S. Kalvoda, B. Paulus, P. Fulde, and H. Stoll, Phys. Rev. B **55**, 4027 (1997).

[7] S.-H. Wei and A. Zunger, Phys. Rev. B **60**, 5404 (1999).

[8] S. R. Kurtz, L. R. Dawson, R. M. Biefeld, D. M. Follstaedt, and B. L. Doyle, Phys. Rev. B **46**, 1909(R) (1992).

[9] V. Dixit, B. Bansal, V. Venkataraman, H. Bhat, and G. Subbanna, Appl. Phys. Lett. **81**, 1630 (2002).

[10] S. Q. Wang and H. Q. Ye, J. Phys.: Condens. Matter **14**, 9579 (2002).

[11] K. Hachelafi, B. Amrani, F. E. H. Hassan, and S. Hiadsi, in *Advances in Condensed Matter Physics*, edited by A. H. Reshak (Research Signpost, Kerala, India, 2009), pp. 1–27.

[12] R. Mohammad and S. Katicioglu, J. Alloys Compd. **469**, 504 (2009).

[13] D. E. Aspnes and A. A. Studna, Phys. Rev. B **27**, 985 (1983).

[14] S. H. Rhim, M. Kim, A. J. Freeman, and R. Asahi, Phys. Rev. B **71**, 045202 (2005).

[15] D. Singh and L. Nordstrom, *Planewaves, Pseudopotentials, and the LAPW Method* (Springer, Berlin, 1994).

[16] S. Blügel and G. Bihlmayer, in *Computational Nanoscience: Do It Yourself!*, edited by J. Grotendorst, S. Blügel, and D. Marx, John von Neumann Institute for Computing NIC Series Vol. 31 (John von Neumann Institute for Computing, Jülich, 2006), p. 85.

[17] P. Blaha, K. Schwarz, G. Madsen, D. Kvasnicka, and J. Luitz, *WIEN2K, An Augmented Plane Wave plus Local Orbitals Program for Calculating Crystal Properties* (Vienna University of Technology, Vienna, 2001).

[18] Z. Wu and R. E. Cohen, Phys. Rev. B **73**, 235116 (2006).

[19] P. E. Blöchl, O. Jepsen, and O. K. Andersen, Phys. Rev. B **49**, 16223 (1994).

[20] F. Tran and P. Blaha, Phys. Rev. Lett. **102**, 226401 (2009).

[21] W. Kohn and L. J. Sham, Phys. Rev. **140**, A1133 (1965).

[22] J. P. Perdew and Y. Wang, Phys. Rev. B **45**, 13244 (1992).

[23] J. P. Perdew, K. Burke, and M. Ernzerhof, Phys. Rev. Lett. **77**, 3865 (1996).

[24] L. Vegard, Z. Phys. **5**, 17 (1921).

[25] N. Peyghambarian, S. Koch, and A. Mysyrowicz, *Introduction to Semiconductor Optics* (Prentice-Hall, Upper Saddle River, NJ, 1993).

[26] S. Namjoo, A. S. H. Rozatiana, and I. Jabbaric, J. Alloys Compd. **628**, 458 (2015).

[27] M. Yen, R. Peopie, K. Wecht, and A. Cho, Appl. Phys. Lett. **52**, 489 (1988).

[28] Z. M. Fang, K. Y. Ma, D. H. Jaw, R. M. Cohen, and G. B. Stringfellow, J. Appl. Phys. **67**, 7034 (1990).

[29] N. V. Smith, Phys. Rev. B **3**, 1862 (1971).

[30] C. Ambrosch-Draxl and J. O. Sofo, Comput. Phys. Commun. **175**, 1 (2006).

[31] F. Wooten, *Optical Properties of Solids* (Academic, New York, 1972).

[32] M. Rohlfing and S. G. Louie, Phys. Rev. Lett. **81**, 2312 (1998).

[33] L. X. Benedict, E. L. Shirley, and R. B. Bohn, Phys. Rev. B **57**, R9385 (1998).

[34] M. Hass and B. Henvis, J. Phys. Chem. Solids **23**, 1099 (1962).

[35] J. Dixon and J. Furdyna, Solid State Commun. **35**, 195 (1980).